NASA Technical Memorandum 102808

Turbulence and Pressure Loss Characteristics of the Inlet Vanes for the 80- by 120-Foot Wind Tunnel

Michael R. Dudley

October 1990

National Aeronautics and Space Administration

NASA Technical Memorandum 102808

Turbulence and Pressure Loss Characteristics of the Inlet Vanes for the 80- by 120-Foot Wind Tunnel

Michael R. Dudley
Ames Research Center, Moffett Field, California

October 1990

National Aeronautics and
Space Administration

Ames Research Center
Moffett Field, California 94035-1000

SYMBOLS

b inlet contraction local width, m (in)

c vane chord length, m (in)

c_f skin friction coefficient

d vane width, m (in)

e_A hot-wire linearizer output for channel A, v

e_B hot-wire linearizer output for channel B, v

$\frac{f_1}{f_2}$ hot-wire probe diameter to sensing length correction factor, = 1.085

K_u axial velocity proportionality constant, m/s/v (ft/s/v)

K_v lateral velocity proportionality constant, m/s/volts (ft/s/v)

$K_{u'}$ axial turbulence proportionality constant, m/s/volts (ft/s/v)

$K_{v'}$ lateral turbulence proportionality constant, m/s/volts (ft/s/v)

l_0 nominal centerline spacing between vanes, m (in)

P pressure, N/m^2 (lbf/in^2)

ΔP_t total pressure difference, upstream of vanes minus local, N/m^2 (lbf/in^2)

q dynamic pressure, N/m^2 (lbf/ft^2)

Re_c Reynolds number based on chord spacing, $\overline{U}c/\nu$

$\tilde{s}$ dimensionless streamwise distance, s/d

t time, s

$\tilde{t}$ dimensionless time scale, $t\overline{U}_0/d = \int_0^{x/d} \frac{\overline{U}_0}{\overline{U}} d(\frac{x'}{d})$

u, v, w instantaneous fluctuating velocity components in the x, y and z directions respectively, m/s (ft/s)

u', v', w' absolute temporal mean turbulence intensities, $\sqrt{\overline{u^2}}, \sqrt{\overline{v^2}}, \sqrt{\overline{w^2}}$ in the x, y and z directions respectively, m/s (ft/s)

$\overline{u'}, \overline{v'}, \overline{w'}$ relative mean turbulence intensities, averaged across two vane spaces,

$$\frac{1}{2l_0\overline{U}^2}\int_{-l_0}^{+l_0} Uu'dy \quad \frac{1}{2l_0\overline{U}^2}\int_{-l_0}^{+l_0} Uv'dy \quad \frac{1}{2l_0\overline{U}^2}\int_{-l_0}^{+l_0} Uw'dy$$

in the x, y and z directions respectively

U, V, W time averaged velocity components in the x, y and z directions respectively, m/s (ft/s)

$\overline{U}, \overline{V}, \overline{W}$ velocity components averaged across two vane spaces,

$$\frac{1}{2l_0}\int_{-l_0}^{+l_0} Udy \quad \frac{1}{2l_0}\int_{-l_0}^{+l_0} Vdy \quad \frac{1}{2l_0}\int_{-l_0}^{+l_0} Wdy$$

in the x, y and z directions respectively, m/s (ft/s)

x, y, z axial, lateral and vertical coordinates, positive aft, right and up, m (in)

$\tilde{x}, \tilde{y}$ dimensionless axial and lateral distance, x/d and y/d

Greek Symbols:

δ boundary height, mm

δ^* boundary layer displacement thickness, mm $\frac{1}{U_1}\int_0^{\delta}(U_1 - u)\,dy_1$

δ^{**} boundary layer momentum thickness, mm $\frac{1}{U_1^2}\int_0^{\delta} u(U_1 - u)\,dy_1$

η mass averaged pressure loss coefficient, $\frac{1}{2l_0\overline{U}}\int_{-l_0}^{+l_0} U\frac{\Delta P_t}{q_0}dy$

κ pressure loss coefficient, $\Delta P_t / q_0$

ν kinematic viscosity, m^2 / s (ft^2 / s)

τ volt meter time constant, s

ϕ vane splay angle

Subscripts:

0 contraction inlet station, or vane trailing edge

1 end of constant area passage between vanes, (throat of diffuser section)

a ambient

t total

SUMMARY

A series of wind tunnel investigations were conducted at NASA Ames Research Center to determine the flow characteristics downstream of a set of wind tunnel inlet flow conditioning vanes. The purpose of these tests was to develop an understanding of the flow mechanisms that contributed to the pressure loss and turbulence generated by the vane set. The near-field characteristics and flow field development were investigated with a 1/3 scale two-dimensional model of the vane set at near full-scale Reynolds numbers. In a second series of tests, the global flow field characteristics were investigated by means of a 1/15 scale model of the full vane set and the 5:1 contraction leading to the model's test section. Scale effects due to Reynolds number mismatch were identified, their significance noted and accounted for when possible. Scaling parameters were adopted that allowed predictions of the expected turbulence and pressure distributions in the full-scale wind tunnel test section, based on the small-scale test results. The predictions were found to be in good agreement with actual measurements made in the full-scale facility.

INTRODUCTION

In July 1980, work was started on the modification of the 40- by 80-Foot Wind Tunnel at the NASA Ames Research Center to increase its research capabilities. The new facility, which includes two wind tunnels, is now known as the National Full-scale Aerodynamics Research Complex (NFAC) (fig. 1). The modifications included extending the speed range of the 40- by 80-foot test section to 155 m/sec (300 knots) and adding a second test section 24.4'm (80'ft) high and 36.6 m (120 ft) wide. The new test section can achieve a maximum speed of a 52 m/sec (100 knots), accommodating larger models with reduced test section wall interference. For a more detailed description of the NFAC see references 1-4.

In 1982, changes in the two wind tunnels were begun to improve the level of flow quality in the new test section so that the variation of spatial and temporal dynamic pressure distributions do not exceed a limit of $\pm 0.5\%$ about the mean value. Additionally, the orthogonal components of relative turbulence intensity were to be less than 0.5%. These goals were deemed necessary for the intended use of the facility to conduct powered-lift, rotor, and basic fluid/aerodynamic research.

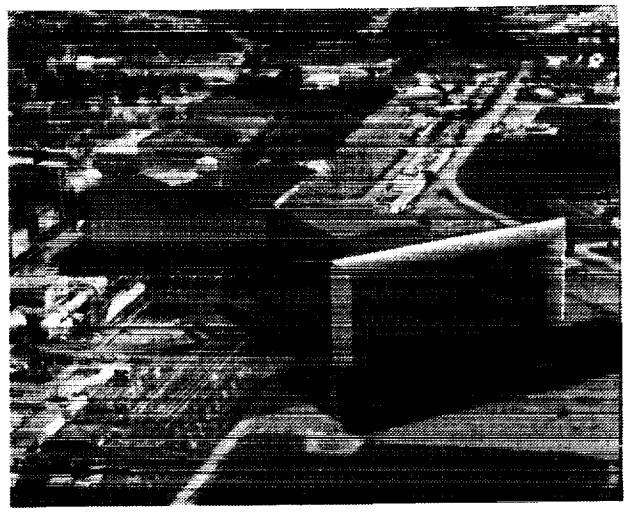

Figure 1. National Full-Scale Aerodynamic Complex, NASA Ames Research Center.

To achieve these objectives, several research programs were initiated to investigate the character of 80- by 120-Foot Wind Tunnel inlet flow and to determine a means to improve the test section flow quality. The programs were both experimental and analytic in nature. The analytic studies made use of data obtained from experimental models to fine-tune their analyses. In many cases the designs of the experimental models were based largely on the results of previous analytic work. This paper deals primarily with the results of two of the experimental investigations that contributed to the overall program.

In 1985, a 1/3 scale two-dimensional model of the new inlet vane set proposed for the 80- by 120-Foot Wind Tunnel was tested in the NASA Ames 7- by 10-Foot Wind Tunnel (fig. 2). (Throughout the paper this investigation will be referred to as the 1/3 scale 2-D test.) The objective of this investigation was to model a segment of the vane set at close to full-scale Reynolds Numbers to obtain accurate measurements of the turbulence generated by, and the pressure loss through, the vane set. These measurements would then establish the initial near-field flow conditions downstream of the vanes. Comparison of these data with similar small-scale measurements allows the identification of scale or modeling differences that might affect the predictions of the behavior of the flow passing through the inlet's contraction to the test section based on small-scale measurements.

The geometry of the proposed vane set and the specifications for the turbulence damping screen attached to its trailing edge were established in a previous study that looked at several modifications to a baseline vane's boat-tail and trailing

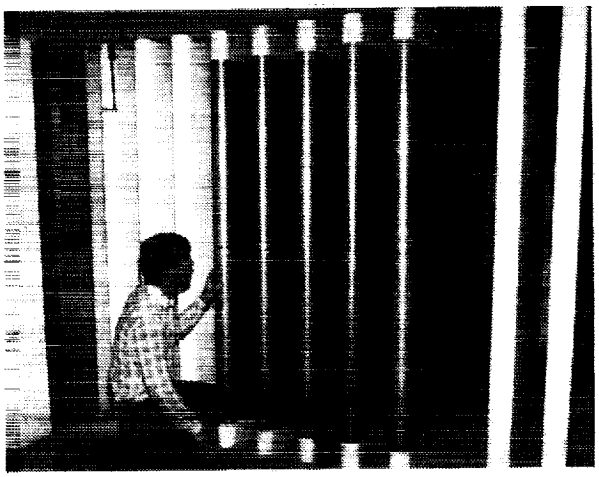

Figure 2. 1/3 scale Inlet Vanes installed in the test section of the NASA Ames 7- by 10-Foot Wind Tunnel.

edge (refs. 5 and 6). The findings of those investigations indicated that, of the configurations tested, the turbulence generated by the vane set could be greatly reduced by doubling the length of the baseline boat-tail and adding a 54% blockage screen to the vane-set trailing edge. This design was adopted for the proposed vane set as the best trade-off in terms of turbulence reduction, reasonable pressure loss, and cost effectiveness. When the model of this design was built for the 1/3 scale 2-D test, it was of sufficiently large scale to simulate the fabrication details that were expected to have an effect on the fluid dynamics of the full-scale problem. This included the surface roughness caused by the vane's perforated metal sides, screen mesh weave and number of wires per cm, and the method of screen attachment to the trailing edge.

In the same year, a 1/15 scale three-dimensional model of the 80- by 120-Foot Wind Tunnel's test section, contraction, and inlet vane set including trailing edge screen was tested at NASA Ames (figs. 3a and 3b). (This investigation will be referred to as the 1/15 scale 3-D test.) Prior to the investigation discussed here, this model underwent several phases of testing to develop a desirable inlet contraction contour, splay distribution (alignment of the inlet vanes relative to the onset flow), and number of horizontal splitter plates. The aim of those studies was to develop a design that would control dynamic pressure in the model test section so that it met the spatial and temporal fluctuation limits. The methodologies used to determine the area and splay distributions and the number of splitter plates adopted for the full-scale wind tunnel design are reported in references 7-10.

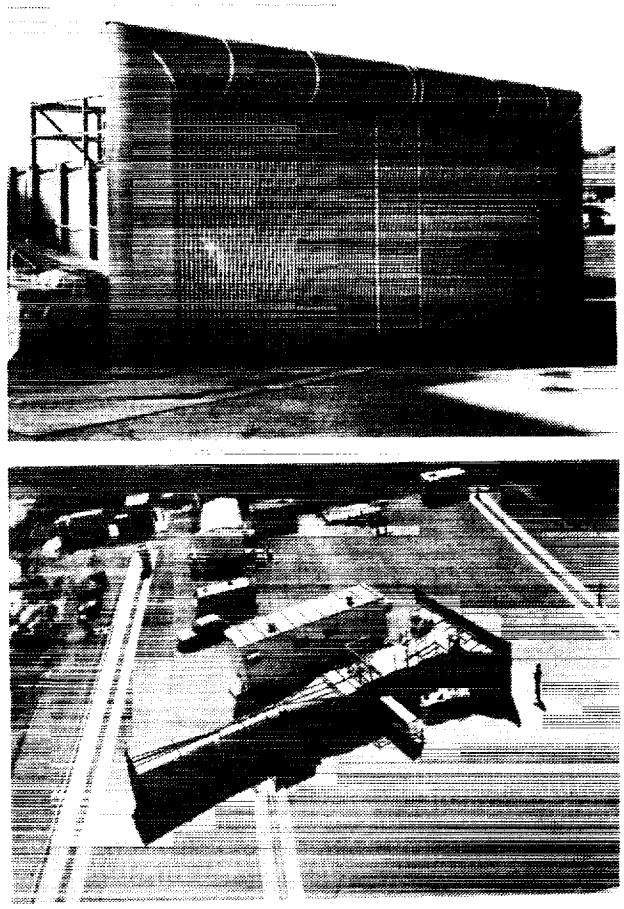

Figures 3a and 3b. 1/15 scale model of the NASA Ames 80- by 120-Foot Wind Tunnel.

The final phase of testing with the 1/15 scale 3-D model is reported here. It describes measurements of turbulence intensity and dynamic pressure inside the model's contraction, downstream of the final vane set design. The objectives of this test were to establish the turbulence decay characteristics and dynamic pressure distribution for the flow as it is conditioned by the inlet contraction. When the appropriate scaling techniques are applied to this information, it allows the prediction of the full-scale wind tunnel test section flow quality. Prior to the construction of the new inlet, these predictions were used to evaluate the effectiveness of the proposed design to reduce the risk of unsatisfactory test section flow quality.

MODEL AND TEST DESCRIPTIONS

1/3 Scale 2-D Test

Model– The model for the 1/3 scale 2-D test consisted of scaled segments of the proposed 80- by 120-Foot Wind Tunnel inlet acoustic baffle vanes. The vanes were constructed of wood with removable sheet metal tails. The bluntness of the

trailing edges was varied by the insertion of wood strips between the closing sides of the of the trailing edges (fig. 4). (Trailing edge bluntness is a requirement of the full-scale design, to allow a point of attachment for the trailing edge turbulence damping screen.)

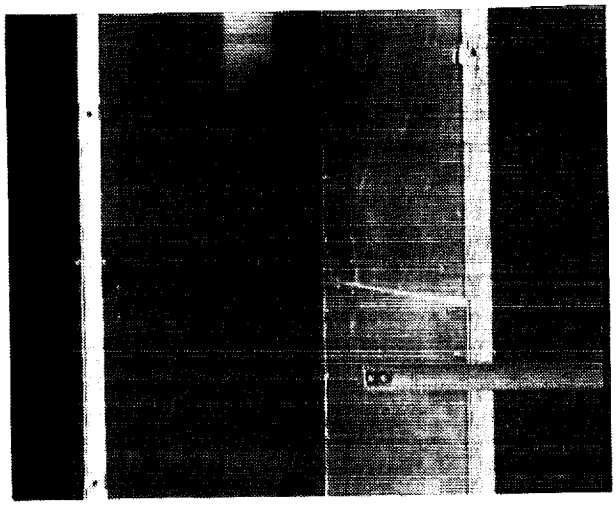

Figure 4. 1/3 scale inlet vane's blunt trailing edges.

Twelve 1/3 scale vane segments of chord, c = 1.626 m, were installed in the Ames 7- by 10-Foot Wind Tunnel test section, spanning from floor to ceiling and forming a vane cascade from wall to wall. Centerline spacing between vanes was l_0 = 22.9 cm. Two half-width vanes were attached to each side wall (figs. 5a and 5b). Flow measurements were restricted to a span of five vane widths, about the center third of the test section and away from the walls, so the model effectively created a two-dimensional representation of a portion of the vane set. Vanes were positioned in the test section by pointed jack screws that penetrated plywood floor and ceiling liners. This provided a convenient means to reposition the vanes within the test section.

The model was tested with and without a 53.8% blockage trailing-edge turbulence damping screen and a 18% blockage, leading-edge bird screen (figs. 6a and 6b). The screens spanned the full width and height of the test section and were of the same type and manufacture as the screens proposed for the full-scale design, (modeled at full, not 1/3 scale). The trailing-edge screen was woven 1.6 mm diameter aluminum wire, 2 wire per cm mesh, double woven (no straight wires). The leading-edge screen was a hot-dipped galvanized 1 mm diameter steel wire, 1 wire per 1.27 cm mesh non-woven (all straight wires).

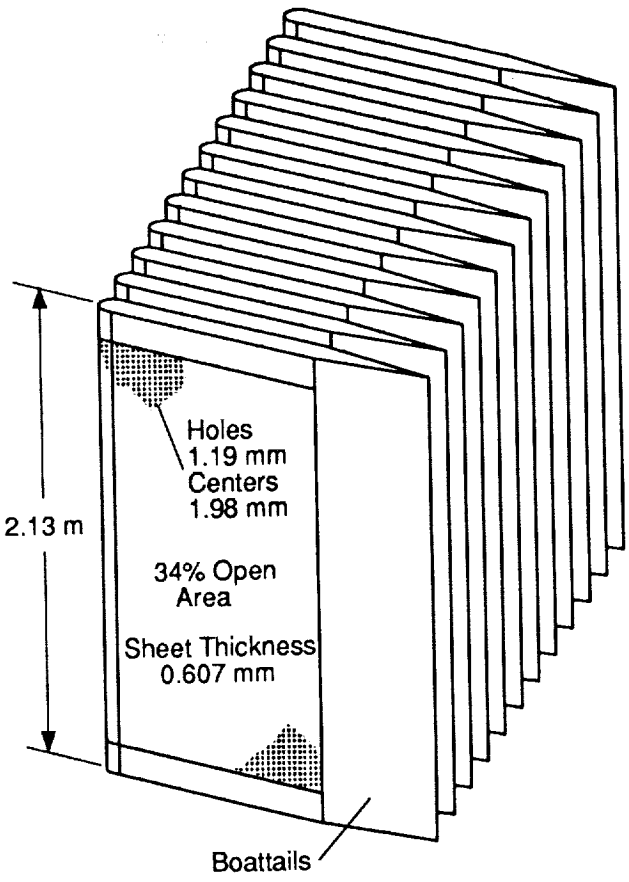

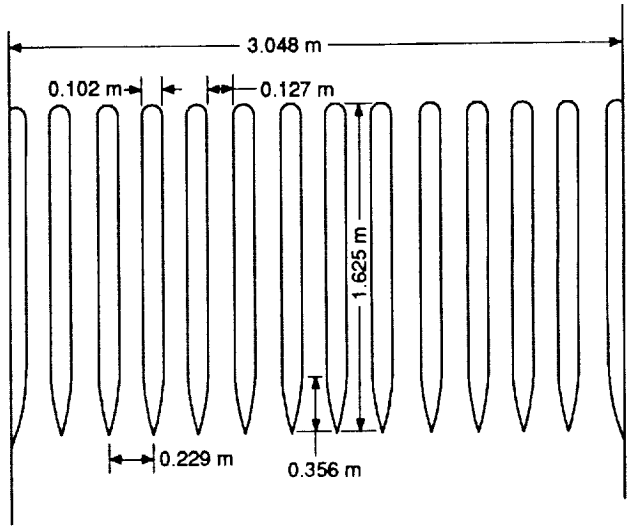

Figures 5a and 5b. Typical installation for 1/3 scale inlet vanes.

The full-scale vanes are constructed with perforated sides for their acoustic damping function. During part of the investigation, the sides of the six center vanes were clad with 0.607 mm thick perforated steel sheets to model surface roughness (figs. 2 and 5a). Because of the dense acoustic backing used inside the full-scale vanes,

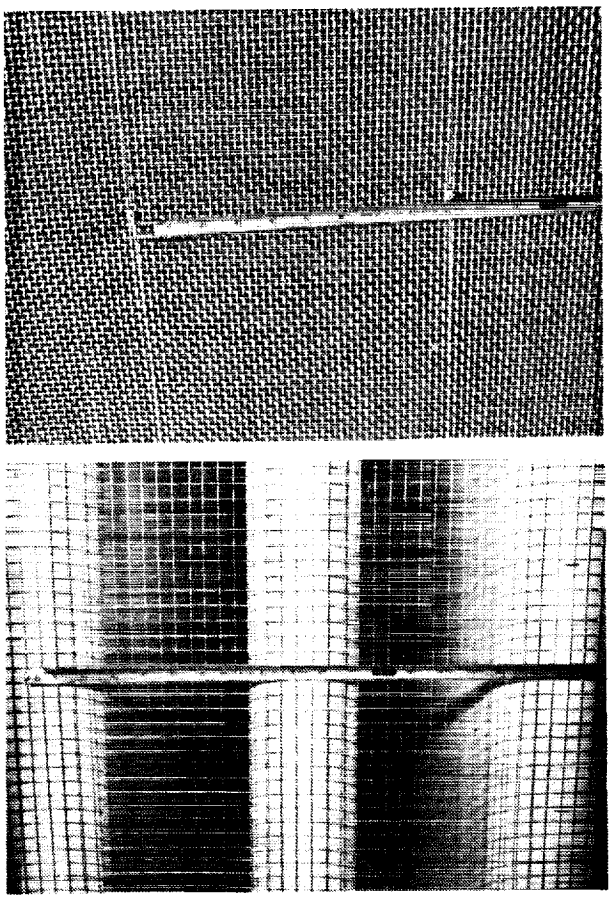

Figures 6a and 6b. Trailing-edge turbulence damping screen and leading-edge bird screen.

there is no significant flow through the surface holes. Likewise, the cladding used on the 1/3 scale model does not allow flow through the holes, but merely simulates the roughness. The 2-D model uses the same 34% open area as the full-scale vanes, but the 1.19 mm holes spaced 1.98 mm between centers are at 1/3 scale.

As mentioned above, the full-scale vanes are splayed to align them with the local streamlines (fig. 7a). The vanes located on the tunnel centerline are defined as having zero splay, $\phi = 0$. Vanes off the centerline have splay angles that correspond to the rotation of the vane from a line parallel to the tunnel centerline. For vanes of a given splay angle, ϕ, the local onset flow sees the vanes as being staggered, with the leading and trailing edges forming lines $90 - \phi$ degrees to the flow (fig. 7b). This also means that the flow will encounter the vanes on one side of the cascade before the other side. Due to the variation in splay angle across the face of the full-scale wind tunnel inlet, the flow passages between the vanes had convergence angles from 0.5 to 1.0°. The vanes tested in the 1/3 scale 2-D model were arranged parallel to each other and did not account for the

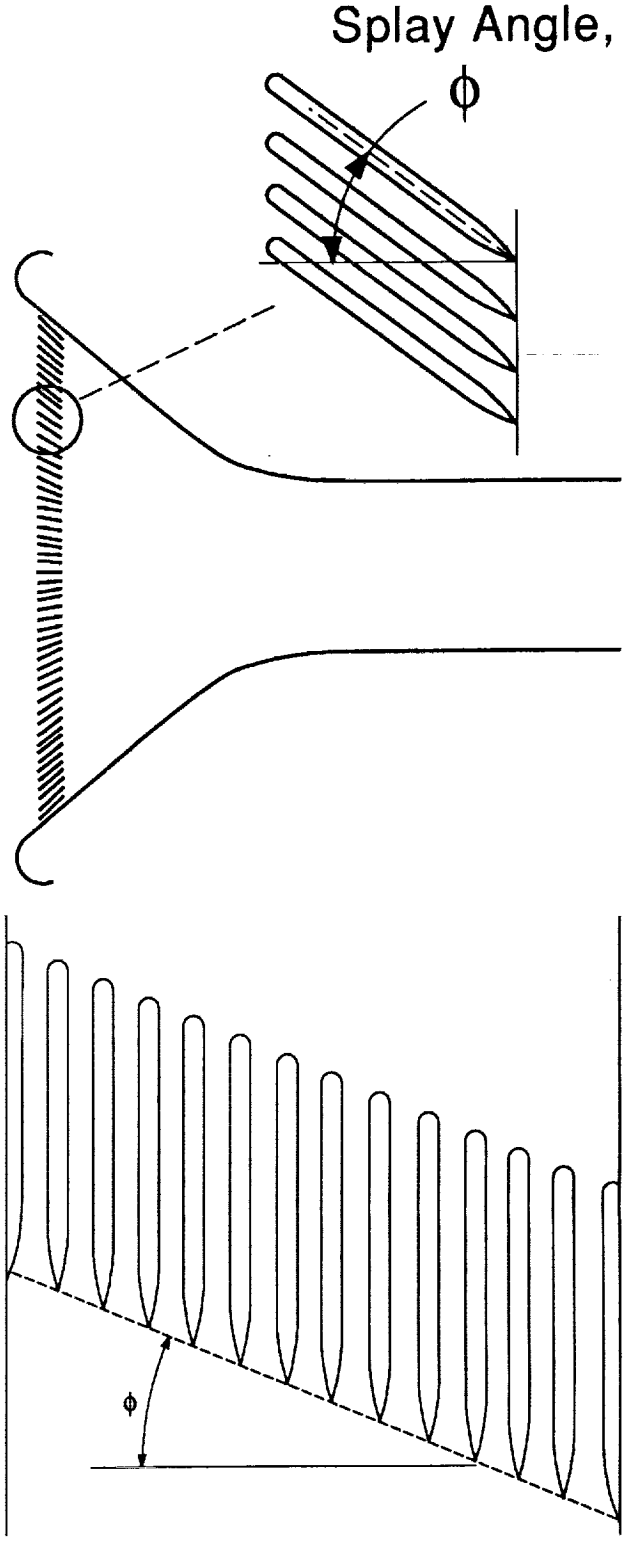

Figures 7a and 7b. Inlet vane splay angles.

slight favorable pressure gradient that exists between the full-scale vanes.

Instrumentation–Velocity and turbulence measurements of the flow field, downstream of the

vane set, were obtained with a two-channel hot-wire anemometer. The hot-wire system consisted of two sets of DISA 55M01 series anemometers, 55D10 linearizers, 55D26 sum-and-difference signal conditioners, 55D31 digital volt meters and 55D35 RMS volt meters. Probes were of the X-wire configuration with 9 μm diameter wires and 2 mm sensitive length. The anemometer is temperature compensated using 55M20 bridge circuits connected to the velocity probe and a second X-wire probe placed in the flow at a very low overheat ratio. A schematic diagram of the basic system is shown in figure 8. Detailed descriptions of the characteristics of this equipment are contained in references 11 and 12.

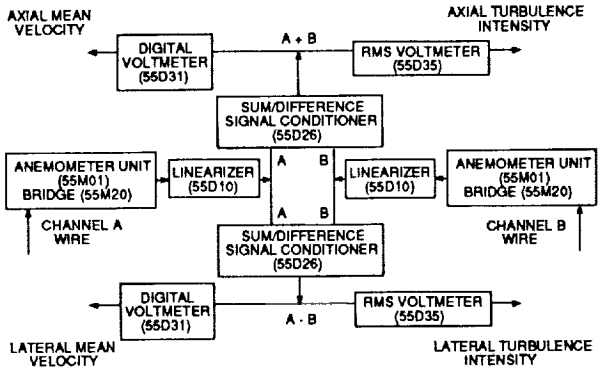

Figure 8. Hot-wire anemometer block diagram.

Linearity checks and linearizer coefficients were determined with a DISA 55D90 calibration unit. Axial velocity was calibrated as a linear function of the sum of the output from the two sensing wires, $(e_A + e_B)$. Lateral velocity was calibrated as a linear function of the difference between the output of the two wires, $(e_A - e_B)$ (refs. 13 and 14). Temporal mean velocities were obtained by digital volt meter (DVM) measurements of the linearized $e_A + e_B$ and $e_A - e_B$ outputs. A DVM time constant setting of τ = 0.3 sec was used throughout the investigation.

Mean velocities were taken to be

$$U = \frac{K_u}{\tau}\int_0^\tau (e_A + e_B)\,dt$$

$$V = \frac{f_1}{f_2}\frac{K_v}{\tau}\int_0^\tau (e_A - e_B)\,dt$$

Absolute turbulence intensities were obtained from RMS volts meters, using a τ = 1.0 sec time constant and interpreted as

$$u' = \frac{K_{u'}}{\tau}\int_0^\tau \sqrt{(e_A + e_B)^2}\,dt$$

$$v' = \frac{f_1}{f_2}\frac{K_{v'}}{\tau}\int_0^\tau \sqrt{(e_A - e_B)^2}\,dt$$

where $K_u, K_v, K_{u'}, K_{v'}$ are calibrated proportionality constants, and $\frac{f_1}{f_2}$ is a correction for the hot-wire probe sensing length to diameter ratio (refs. 13-15).

The local total pressure drop through the vane set, ΔP_t, was measured with a 1.59 mm diameter pitot probe downstream of the vanes and referenced to the total pressure orifice of the pitot-static probe upstream of the vane set. Test section dynamic pressure upstream of the model, q_0, was measured by both the standard 7- by 10-Foot Wind Tunnel static pressure orifices and a pitot-static probe. Measurements of ΔP_t and q_0 were made with 6.9 KPa (1.0 psid) Druck pressure transducers. Pressure transducer calibrations prior to the test were found to be linear and repeatable to within 0.1%. Standard deviation of the errors were less than 0.01%.

Hot-wire velocity and ΔP_t probes were mounted on an extension to the tip of a boom supported by a horizontally driven survey apparatus (figs. 9a and 9b). A stepper motor was used to drive the boom lateral to the free stream. Linear position accuracy of the boom mount was 0.05 mm. The resulting lateral probe position accuracy was 0.5 mm, due to clearance tolerances of the boom support. Vertical position of the probe was maintained at a constant height with a total variation less than 4.0 mm for a typical traversing survey spanning 1.0 m. The mean vertical position of the probe varied from traverse to traverse, but was always within 10% of the mid-height of the test section. The vertical position of the ΔP_t probe was 5.0 cm above the hot-wire probe. Axial position of the probes was adjusted manually, either by extending and retracting the boom relative to the traversing platform, or to reposition the entire survey apparatus to a different downstream location. Axial position accuracy was to within $\pm$2.0 mm over a 1.0 m span, measured from the trailing edge of the vane set.

Survey apparatus stepper-motor control and analog-to-digital signal conditioning were accomplished with a Hewlett Packard 6942A multi-programmer. The multi-programmer in turn was controlled by an H.P. 9836 micro-computer that was also used for data reduction. Velocity, turbulence intensity, and pressure loss data were recorded with X-Y pen plotters versus spanwise

ORIGINAL PAGE
BLACK AND WHITE PHOTOGRAPH

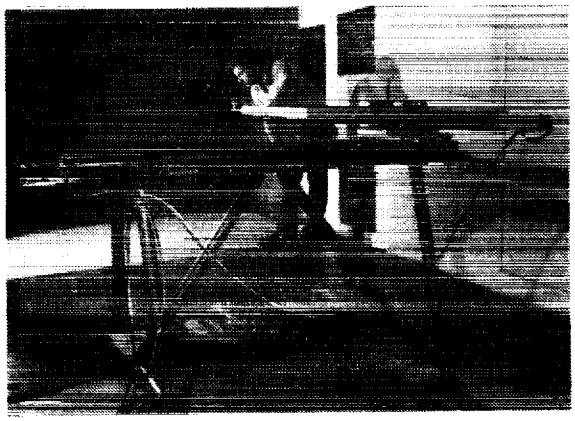

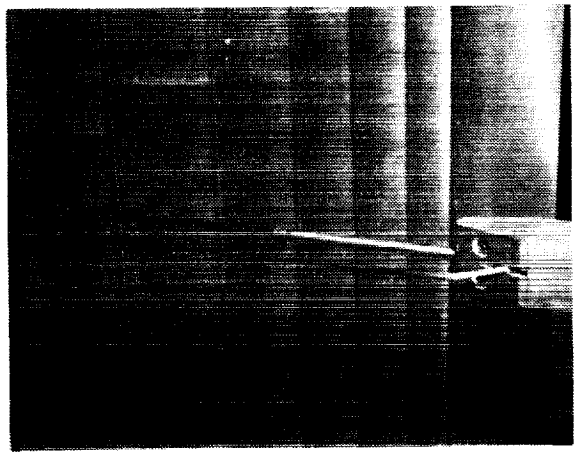

Figures 9a and 9b. Traversing survey apparatus and probe.

position. Analog signals from the anemometers, pressure transducers, and survey position, along with a 1-kHz reference signal, were recorded on an Ampex 14-channel tape recorder for post-run playback. Selected points in the flow were also sampled with an H.P. two-channel narrowband spectrum analyzer to determine the frequency distribution of the flow's turbulent energy.

Test conditions and flow surveys– When the 80- by 120-Foot Wind Tunnel test section is at its maximum speed of 52 m/sec (100 knots), the inlet nominal onset velocity is about 10 m/sec (20 knots). This speed varies across the face of the inlet, with the maximum being at the center and the minimum at the edges. All testing of the 1/3 scale model was done at 30 m/sec to match the full-scale Reynolds numbers based on vane cord length, $Re_c = 2.23 \times 10^6$.

The parameters varied for the model configurations investigated were: simulated vane splay angles, (ϕ = 0°, 7°, 20°, and 40°), the presence of leading- and/or trailing-edge screens, perforated sheet-metal cladding on the center six vanes, and trailing-edge thickness (2, 10, and 14 mm).

Boundary layer surveys were made in one of the passages between two vanes using a single-channel hot-wire probe with an offset sensing element designed for measurements close to a wall. The axial location of the boundary layer surveys was the throat of the diffuser formed by adjacent boat-tails. Surveys were made for both smooth and rough walls, but never in the presence of the trailing-edge turbulence damping screen.

Traversing surveys made downstream of the vane trailing edges spanned $\pm 2.5\ l_0$ about the center of the test section. For the 1/3 scale test the vane spacing was l_0 = 0.229 m. Data samples were taken every 6.35 mm. The axial stations of these traverses, measured from the trailing edge nondimensionalized by the vane width (d = 0.102 m) were $\tilde{x}$ = 0.07, 2.25, 4.5, 9.0, 18.0, and 27.0. For the traverses made behind the configurations with simulated vane splay, the boom was maintained aligned with the flow, but the traverse path was at an angle $(90 - \phi)$ degrees to the flow, parallel to the vane trailing edges. In this way, the probe was keep a constant streamwise distance from the vane-set trailing edge.

Discrete point measurements of turbulence spectra were made at the same axial stations as the traverses, but positioned either directly behind a vane's centerline, or behind the center of the passage between two vanes.

1/15 Scale 3-D Test

Model– The 1/15 Scale 3-D model is a functioning replica of the 80- by 120-Foot Wind Tunnel. The model is powered by a 2.0 m diameter, 895 kw electric fan drive, and has a test section 1.62 m by 2.44 m. The 1/15 scale 3-D wind tunnel modeled the final design chosen for the inlet vanes, the contraction and the test section, but the geometry of the 80- by 120-Foot Wind Tunnel downstream of the test section was not duplicated (figs. 3a, 3b, and 10). The inlet vanes had a chord of c = 32.5 cm, and a nominal centerline spacing of l_0 = 4.57 cm. Vane splay angles varied from $\phi = 0°$ at the inlet centerline to $\phi = 42°$ at the wall. No vane surface roughness was simulated for this test. A 53.8% blockage turbulence damping screen was attached to the trailing edge of the vane set, with no simulated trailing-edge bluntness. This screen was 8 wire per cm mesh with 0.41 mm diameter wires and was 1/4 of full-scale. The same type 18% blockage leading-edge bird protection screen as was used for the 1/3 scale test, was also used for this test and is the same as proposed for the full-scale wind tunnel

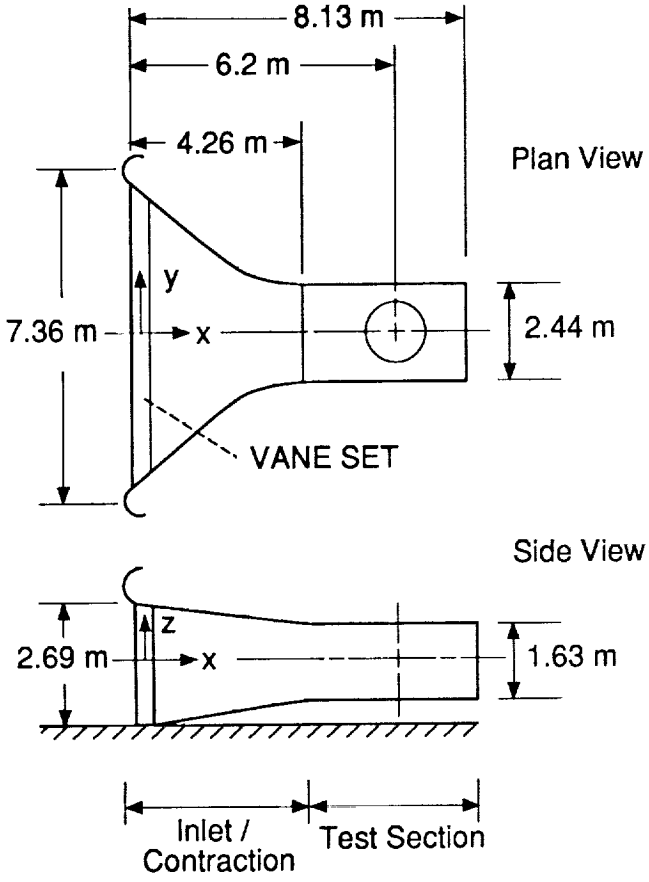

Figure 10. Diagram of 1/15 scale model of the 80- by 120-Foot Wind Tunnel Inlet, Contraction and Test Section.

(hot dipped galvanized 1 mm diameter steel wire, 1 wire per 1.27 cm mesh non-woven screen).

Instrumentation– The same survey apparatus, hot-wire anemometer system, and ΔP_t probe that were used to measure the flow field in the 1/3 scale test, were also used in this investigation. The only differences were that the pressure transducers were referenced to ambient pressure, P_a, two inlet diameters ahead of the inlet instead of test section total pressure, and that DISA 55M10, non-temperature-compensated bridge circuits were used with the hot-wire anemometers. To monitor ambient wind conditions in the vicinity of the inlet, a cup-type wind anemometer and wind direction vane were placed at the same location as the P_a sensing tap.

Test conditions and flow surveys– No changes were made to the model during this phase of the investigation. The only parameter varied was test-section velocity. All flow surveys were conducted with test-section velocities of either 42 or 21 m/sec. At maximum power, the 1/15 Scale Wind Tunnel was capable of a test section velocity of 42 m/sec. The Reynolds numbers based on vane chord length for the two test conditions were $Re_c = 1.83 \times 10^5$ and $Re_c = 9.15 \times 10^4$.

The entire investigation consisted of flow surveys of velocity, turbulence, and total pressure in the contraction and test section of the 1/15 scale model. Axial locations of the traversing surveys, nondimensionalized by vane width and measured along contraction streamlines, were $\tilde{s}$ = 1.1, 6.8, 13.5, 27.0, 54.0, 81.0, 108, and 216. The station $\tilde{s}$ = 216 is located at the beginning of the test section. The vertical positions of the surveys were constant for any particular traverse, but varied from 15% of the duct height below centerline near the vane set, to 7% above centerline in the test section. The spanwise position of the surveys was located to sample the flow along specific streamlines. Streamlines of interest were ones that originated from vanes having splay angles of 1°, 7°, 20°, or 40° (fig. 11). The 1° streamline was chosen rather than 0° due to inlet support structure on the tunnel centerline (ref. 9). Surveys spanned a lateral distance of 25.4 cm, approximately $\pm 2.5\ l_0$ at 1/15 scale, for $\tilde{x} \leq 62$. Surveys at $\tilde{x}$ = 108 and 216 spanned $\pm 12\ l_0$ about the tunnel centerline.

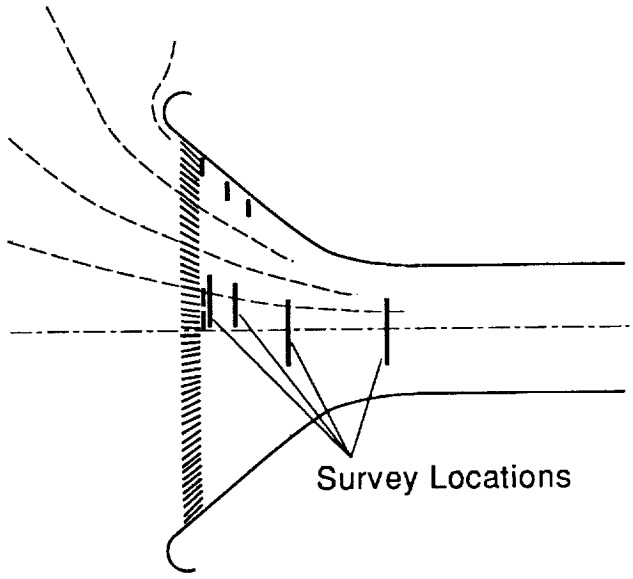

Figure 11. Locations of spanwise surveys.

RESULTS AND DISCUSSION

The primary goals of this investigation were to predict the turbulence levels expected in the 80- by 120-foot wind tunnel test section and to determine inlet vane pressure losses. The pressure loss information was required as an input

to other analyses aimed at predicting test section spatial velocity distributions (ref. 8). The first step of the strategy adopted for this investigation was to compare the 1/3 scale near field wake characteristics ($\tilde{x} < 30$) to the near field measurements made in the 1/15 scale test, and to published data of cascades of planar-type wakes. Next, having established the similarities and differences between the full-scale, small-scale, and published wakes, predictions of the far field behavior ($\tilde{x} > 20$) could be made by application of published data and 1/15 scale test data. The confidence level of these predictions depends on the degree to which measured full-scale properties were matched by the small-scale data, and measurements reported in the literature.

One difficulty encountered when comparing the 1/15 scale inlet contraction data to 1/3 scale data, and to previous studies conducted using constant flow area ducts, was the choice of an appropriate variable to define downstream position. The most commonly used parameter to define downstream position in wake decay studies is a dimensionless streamwise distance, $\tilde{x} = x/d$. Since wake decay properties are temporal, as well as spatial, the use of this parameter presupposes an unchanging $\overline{U}$. For duct flows with a changing mean velocity due to a nonuniform flow area, the dimensionless time scale,

$$\tilde{t} = t\,\overline{U}_0/d = \int_0^{x/d} \frac{\overline{U}_0}{\overline{U}} d\left(\frac{x'}{d}\right)$$

used by Comte-Bellot and Corsin, is more appropriate (ref. 16; note x' is a dummy integrating variable). When the duct area is constant, $\overline{U}_0/\overline{U} = 1.0$ and the integral reduces to $\tilde{t} = x/d = \tilde{x}$. Values of $\tilde{t}$ for the 1/15 scale test were determined by integrating a fourth-order polynomial curve fit of the experimentally measured values of $\overline{U}_0/\overline{U}$ (fig. 12). Calculation of $\tilde{t}$ along streamlines on the centerline and $\phi = 20°$ use the same polynomial coefficients. A separate set of coefficients is used for the $\phi = 40°$ data. The inlet face to test section velocity ratio of 0.275 implies that the effective inlet contraction ratio is 3.64:1, less than the geometric contraction ratio of 5:1.

Near Field Characteristics

Baseline vane set characteristics– Prior to testing the vane set with leading- and trailing-edge screens installed, a baseline set was tested with no screens. This was done to establish the character of a minimum vane set and confirm the requirement for screens to manage wake turbulence intensity. Figure 13 is a series of axial and

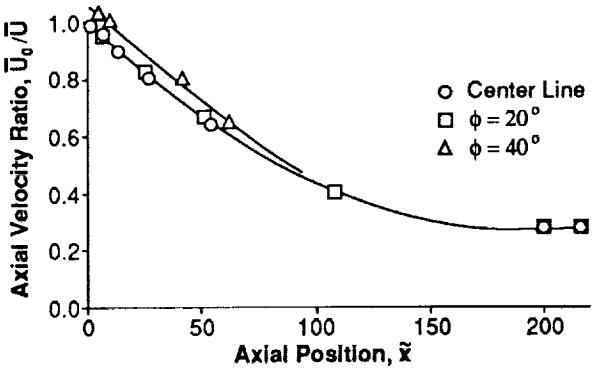

Figure 12. 1/15 scale wind tunnel contraction mean axial velocity ratio.

lateral velocity profiles. All profiles are shown spanning two wakes, over a range of $\pm y/l_0$, centered about the channel between two vanes. The profiles start very near the vane trailing edges, $\tilde{t} = 0.07$, and proceeding downstream to $\tilde{t} = 27.0$. Figure 14 is the series of axial and lateral turbulence intensity profiles at the same downstream locations.

Velocities are non-dimensionalized by the spatially averaged mean axial velocity $\overline{U}$. The axial velocity profiles are similar to those observed behind parallel circular rods (refs. 17 and 18). The primary difference between the wakes of a vane set and a cascade of circular rods of the same solidity, is that the delayed separation on the vane boattails creates a narrower wake and wider region of high velocity flow between the vanes. At the station $\tilde{t} = 18$, downstream of the baseline vane set, the axial flow is essentially uniform. For measurements behind parallel rods, the flow is usually considered to be established as uniform and homogeneous by $\tilde{t} > 20$. Repeated measurements of $U/\overline{U}$ profiles, not shown here, indicate the perturbations about $\overline{U}$ are temporal and of the order of $0.5\ u'/\overline{U}$. Lateral velocity measurements show about the same unsteadiness. Note that lateral velocity measurements indicate a mean flow of $V/\overline{U} = -0.1$ (to the left looking upstream) which is about 6° or half the vane boattail closure angle. Flow to the left is consistent with the observed shift of the peak values of $U/\overline{U}$.

Tuft-type flow visualization revealed the lateral flow to be caused by a nonsymmetric flow separation in the the diverging passage between the vane boattails. By referring to a two-dimensional diffuser performance chart (ref. 19), it can be seen that the passage created by the boattail geometry is a relatively wide angle diffuser, where transitory separation off one wall is expected. For the majority of the test, flow stayed

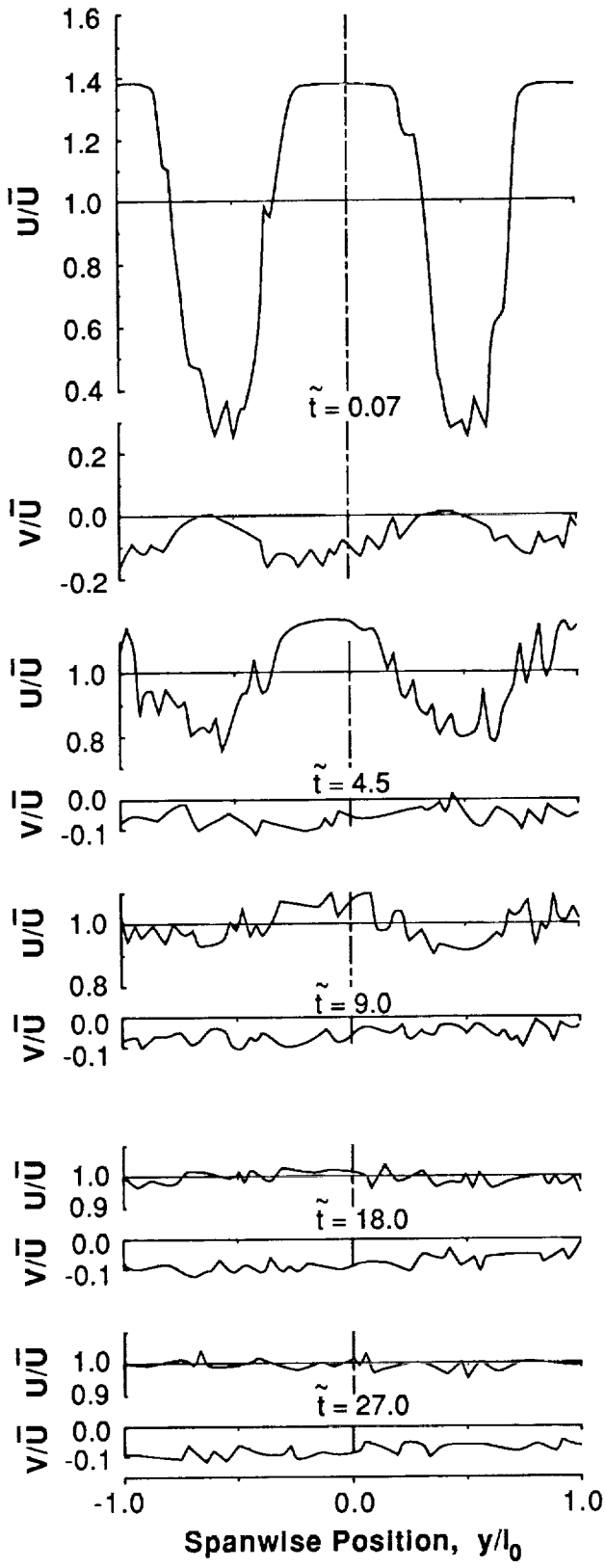

Figure 13. Axial and lateral mean velocity profiles, 1/3 scale data, no screens.

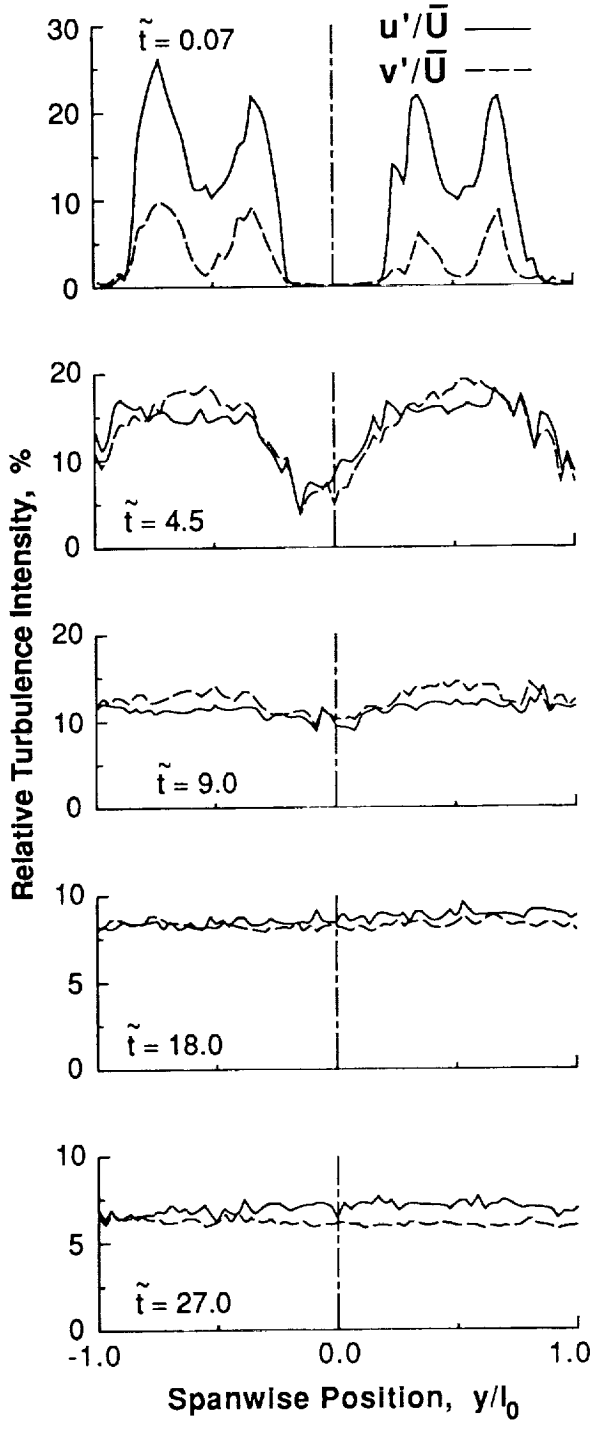

Figure 14. Axial and lateral turbulence intensity profiles, 1/3 scale data, no screens.

attached to the left side of the passage and separate on the right. This condition in one channel tends to enforce the same bias in all channels of the vane set. Occasionally the reverse was observed, with all channels separating to the right. Once established, the direction of separation would persist for long periods of time. The large values $V/\overline{U}$ and the bi-modal nature in which they can be created over significant portion of the face of the inlet makes this a highly undesirable characteristic for a flow-conditioning vane set.

The profiles of turbulence characteristics are also typical of parallel rods or bars. Initial intensities are high and anisotropic with u' being greater. The notch in the intensity profile at the center of the wake for $\tilde{t} = 0.07$ is exaggerated because turbulence intensity is nondimensionalized by $\overline{U}$, which is averaged over the entire span of the profile. Turbulence intensities in regions of low mean velocity will appear to be less than if they were scaled by local mean velocity.

By the time the flow has reached $\tilde{t} = 18.0$ it is homogeneous and isotropic. Experimental and theoretical studies have shown that during the initial period of decay, $20 < \tilde{t} < 150$, the turbulence intensities in a homogeneous isotropic flow field downstream from a grid or parallel rods will decay according to

$$u' \propto \tilde{t}^{-n}$$

where n is in the range $0.5 < n < 1.0$ (refs. 16 and 20-22). By combining the 1/3 scale test data with this function, an estimate can be made of turbulence intensities in a test section downstream from a baseline vane set.

The initial decay of the spatially averaged axial and lateral turbulence intensities, $\overline{u'}$, $\overline{v'}$, downstream of the baseline vane set, are plotted in figure 15. A line of slope -0.71 is also plotted, extrapolating the data to $\tilde{t} = 127$, the test section location. The exponent $n = 0.71$ is the experimental value for a cascade of parallel rods, solidity equal to 0.38 (ref. 22). The extrapolation predicts $\overline{u'} = 2.1\%$ at $\tilde{t} = 127$ if $\overline{U}$ remains constant. The relative turbulence intensity will be further decreased by the accelerating mean flow. Multiplying $\overline{u'}$ by the inlet face to test section velocity ratio, $\overline{U}_0/\overline{U}_{ts} = 0.275$ taken from figure 12, the estimate becomes $\overline{u'} = 0.6\%$. Experimental observations have shown that converging ducts with contraction ratios greater than 1:1.3 reverse the relative turbulence anisotropy making $v' > u'$ (refs. 17 and 23). This, coupled with the slower decay rates usually observed for lateral turbulence intensity, would lead one to expect values of $\overline{v'} > 0.6\%$ in the test section. The prediction of values greater than the the desired specification of $\overline{u'}$ and $\overline{v'} < 0.5\%$, and the significant lateral mean velocities generated by the vane set, confirm the need for some form of flow separation and turbulence management device.

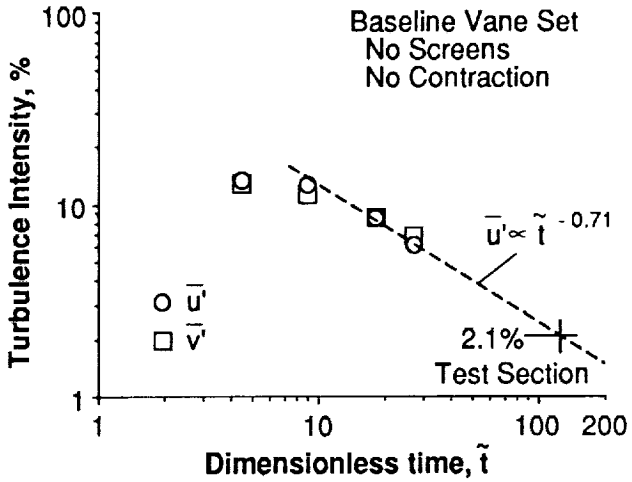

Figure 15. Axial and lateral turbulence intensities, 1/3 downstream of baseline vane set.

Characteristics of proposed vane set– It is well known that a series of screens downstream of a cascade, each separated by several hundred screen mesh diameters, is an efficient method to reduce the scale of the turbulence generated by the cascade and help isolate an open circuit wind tunnel from meteorological turbulence (ref. 24). However, because of the size of the NFAC, cost and installation complexity considerations limited the design options to a single trailing edge screen. As previously mentioned, a 54% blockage screen is attached to the trailing edge of the proposed vane set. The trailing-edge thickness of the 1/3 scale vanes is blunted to 14% of the vane thickness to simulate the the full-scale screen installation (fig. 4). The vanes are also clad with perforated sheet-metal skins to simulate the full-scale surface roughness, and a coarse bird screen is attached to the leading edges.

A series of velocity and turbulence intensity surveys of the proposed vane set, measured at the same spanwise and downstream locations as the baseline data presented in figures 13 and 14, are shown in figures 16 and 17. The primary difference between these wake velocities and the baseline is that the velocity deficits are

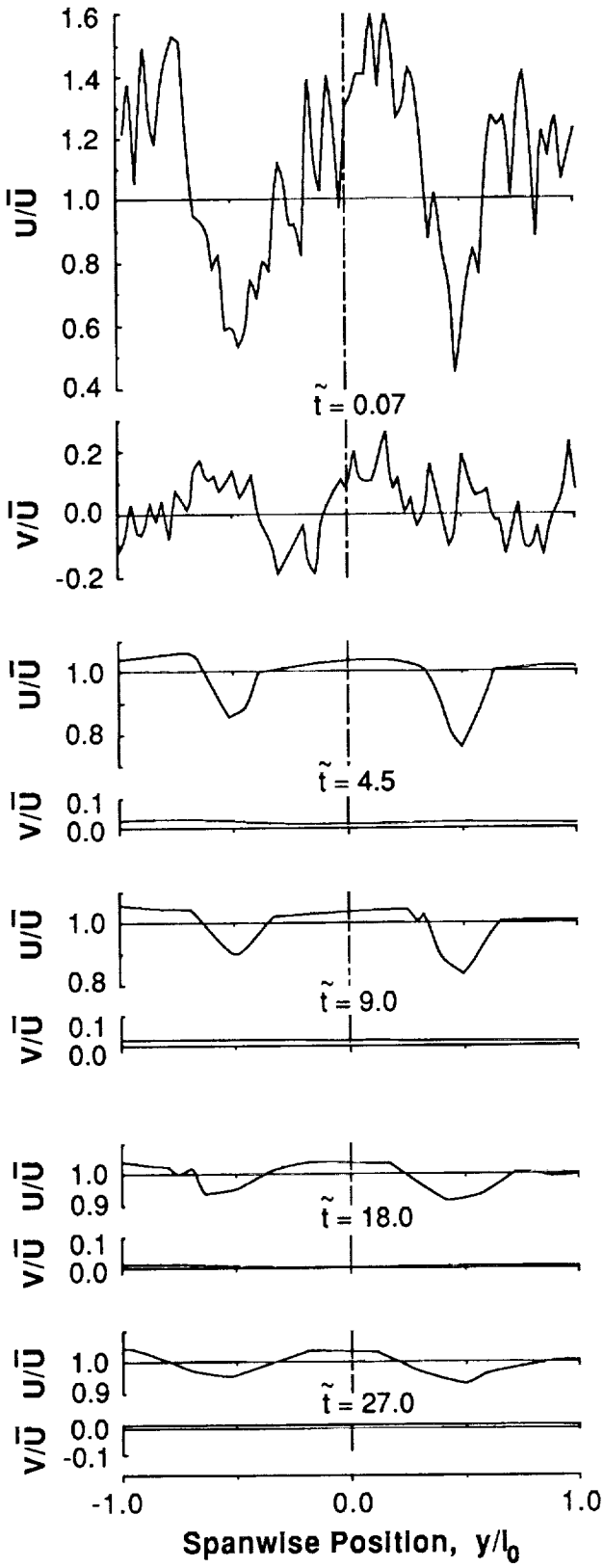

Figure 16. Axial and lateral mean velocity profiles, 1/3 scale data, with screens.

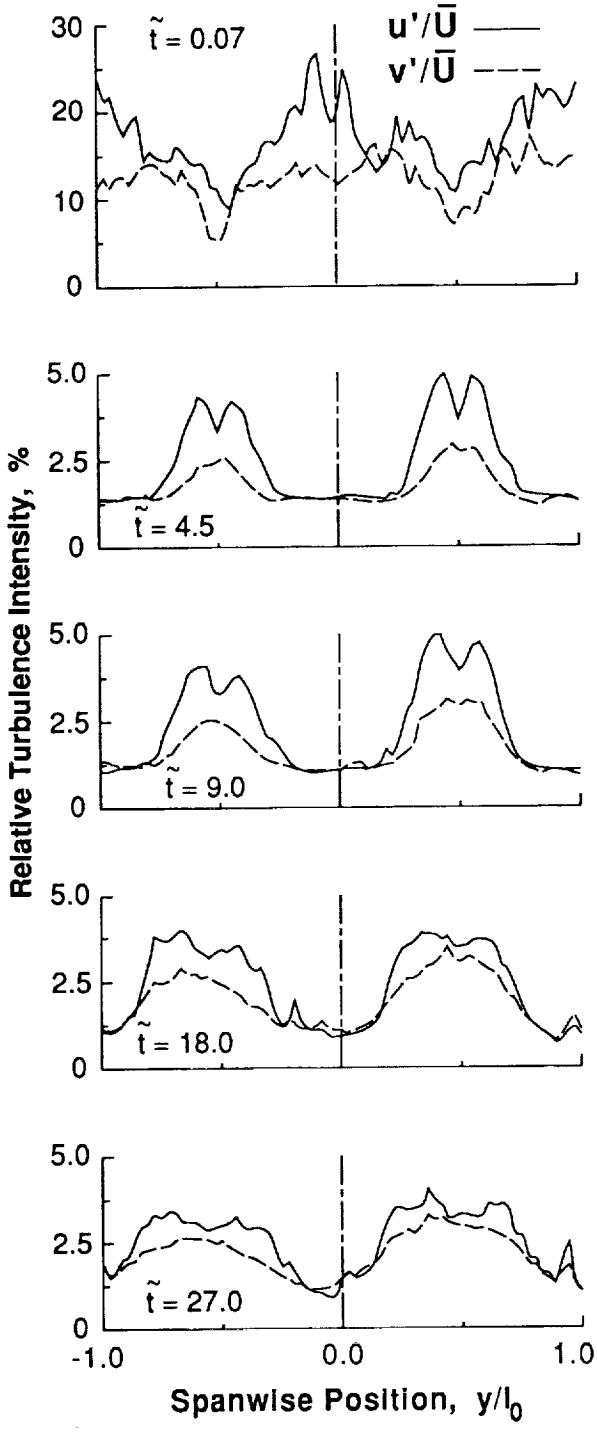

Figure 17. Axial and lateral turbulence intensity profiles, 1/3 scale data, with screens.

smaller but persist longer. This appears to result from a delay in the interactions between adjacent wakes that would normally produces a homogeneous turbulence field by $\tilde{t}$ = 20. Examination of the turbulence profiles reveals that the delay is caused by a buffer region of low turbulence between the wakes and initially low values of v' caused by the trailing edge screen. Higher values of v' would accelerate the lateral convection of turbulence between the wakes and reduce the time necessary to establish a homogeneous flow field. There is very little reduction in u' until the wakes start to become isotropic and merge. It is also worth noting that the screen's ability to "backfill the diffuser"has helped control separation on the vane boattails and eliminate any significant lateral velocities. The use of screens to back fill diffusers is discussed in reference 25.

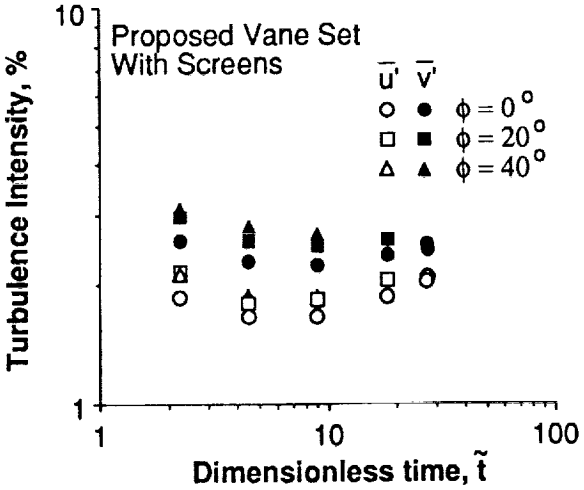

Figure 18. Turbulence intensity for various splay angles, downstream of 1/3 scale vane set.

For vanes located off the wind tunnel centerline, the cascade will appear to be staggered to the onset flow (figs. 7a and 7b). A concern is what effect, if any, vane splay angle, ϕ, has on u' and v'. Measurements of $\overline{u'}$ and $\overline{v'}$ at several downstream stations for ϕ = 0°, 20°, and 40° are shown in figure 18. The data indicate there is a slight, but consistent increase in $\overline{u'}$ and $\overline{v'}$ with ϕ. The apparent change in the relative position of the vanes has the effect of modifying the flow passage diffuser geometry and the flow mean onset angle to the screen. The diffuser effective area ratio is reduced by the change, and this should help reduce the wake, but the reduced screen head loss due to the stagger angle also reduces its ability to backfill the diffuser and control separation. The net result, as can be seen in figure 19, is higher turbulence levels for increased ϕ.

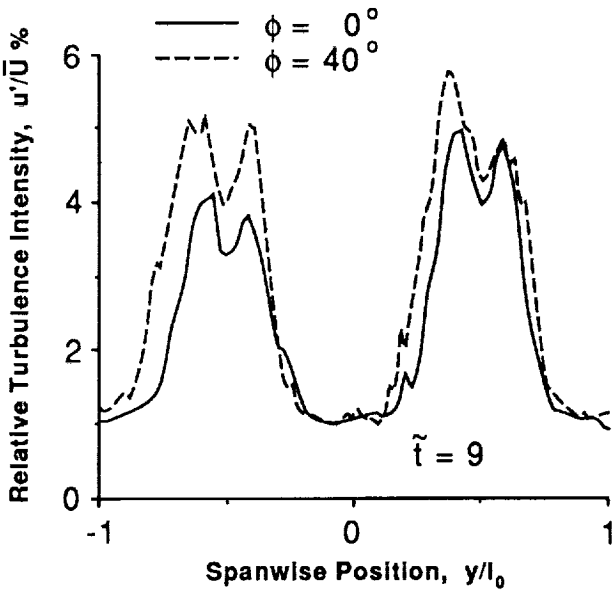

Figure 19. Axial turbulence intensity for two vane splay angles, 1/3 scale data.

This same effect was also observer in the 1/15 scale data. Measurements of $u'/\overline{U}$ made at increasing spanwise locations (increasing ϕ) for a given downstream position increased in magnitude (fig. 20).

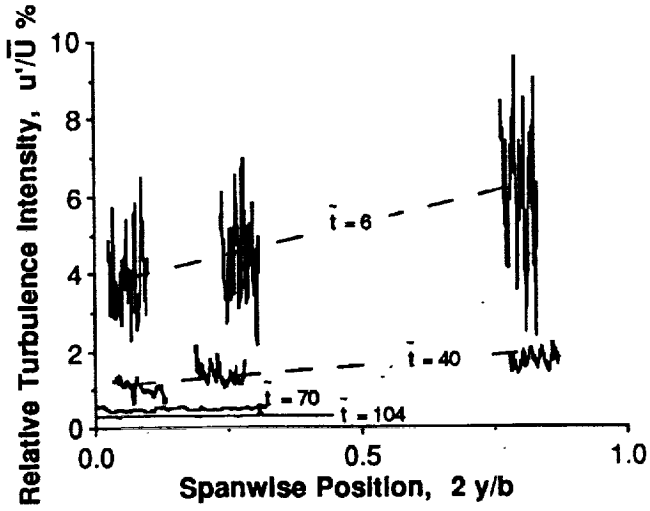

Figure 20. Axial turbulence intensity for various splay angles, downstream of 1/15 scale vane set.

1/3 to 1/15 Scale Data Comparisons

Before discussing the differences in mean and unsteady flow characteristic in the large and small scale experiments, it is important to recognize that there are a few significant geometric features that differ in the experimental hardware

between the two tests. The first and most obvious is the flow downstream of the 1/3 scale vanes is in a constant area duct, as opposed to a converging and accelerating flow in the 1/15 scale model. The small-scale wakes are squeezed as they progress, and if plotted using a constant spanwise length scale, get narrower at each downstream station. By non-dimensionalizing spanwise position by the local contraction width, b, wakes at successive downstream measurements can be scaled to comparable widths.

A second and more subtle feature concerns the matching of dominant turbulence scale lengths. Although no direct measurements were made of turbulence scale, experience indicates that it would be reasonable to expect turbulent scales of the order of the vane thickness and spacing, and smaller scales of the order of the trailing edge screen mesh length. In the large-scale experiment the ratio of these scales is approximately 60:1, but only 20:1 for the small-scale model. The ratio of turbulent scales is known to have an influence rate of turbulence convective mixing, with the maximum mixing occurring when the ratio is about 5:1 (ref. 20).

Vertical mixing in the 1/15 scale model is also enhanced by wakes shed off the horizontal splitter plates. These plates are designed to provide lateral vane support and modify the distribution of the mean flow in the vertical plane. No splitters plates were installed in the two-dimensional model.

Finally, the development of boundary layers in the constant area section between the vanes is controlled by differences in Reynolds numbers and surface roughness; and consequently so is the boundary layer throat blockage at the start of the diffusing section. The throat blockage will affect the diffuser performance, and hence the size of the wakes generated (ref. 26).

The following discussions attempt to address how these differences affect the data and the ability to predict the parameters of interest.

Wake mean flow characteristics– A convenient method of comparing wake mean axial flow profiles, are surveys of the total pressure loss perturbation, $\kappa - \eta$. A quantity based on pressure was chosen for this comparison because the accuracy of pressure measurements are greater than velocity in these experiments. The perturbation is defined by the following two parameters:

$$\kappa = \Delta P_t / q_0$$

the local deficit in total pressure, referenced to the total pressure upstream of the vanes and non-dimensionalized by onset dynamic pressure at the vane set centerline, and

$$\eta = \frac{1}{2 l_0 \overline{U}} \int_{-l_0}^{+l_0} U \kappa \, dy$$

a spatial averaged pressure loss coefficient. It can be shown that

$$\kappa - \eta \approx \left(\frac{U}{\overline{U}}\right)^2 - 1$$

Pressure loss profiles at several downstream locations, covering a span of two wakes slightly to the right of the tunnel centerline, $2y/b = 0.03$ to 0.06, are shown in figure 21. The span of each curve is scaled by a value of b equal to the width of the contraction at the survey location. All of the two-dimensional data shown here uses $b = b_0$, the width of the contraction at the vane set trailing edge. The 2-D data has been shifted laterally so that the vane trailing edge spanwise positions match the locations of the 1/15 scale vanes. These manipulations allows a more direct comparison of the wakes.

The evolution of the near field wake is shown in figure 21a, while figure 21c shows the continuation of the perturbation decay to $\bar{t} = 105$, the position corresponding to the end of the contraction and the beginning of the test section. For clarity, the profiles at the closest match point, $\bar{t} = 27$ and $\bar{t} = 24$, are shown separately in figure 21b. The profiles at this location agree well enough to indicate a good matching of the large- and small-scale mean flow properties. It is interesting that in this example the 3-D profiles are more repeatable from wake to wake than the 2-D data.

Characteristics of turbulence in wake– When the prediction of turbulence decay downstream of the baseline vane set was made by extrapolating the data in figure 15, using an empirical power law decay function, it was assumed that the decay behavior in a contraction and in a constant area duct are similar. A check on the validity of this assumption can be made by examining the turbulence levels in the 1/15 scale model's contraction.

Figure 22 plots $\overline{u'}$ and $\overline{v'}$ along the contraction centerline at several downstream positions. To compensate for the decrease in "relative" turbulence intensity due to the increase in axial mean velocity in the contraction, $\overline{u'}$ and $\overline{v'}$ are scaled by the mean velocity at the beginning of the contraction, $\overline{U}_0$, instead of the local mean velocity $\overline{U}$. The empirical decay function for round parallel rods from figure 15 is replotted in figure 22 for reference.

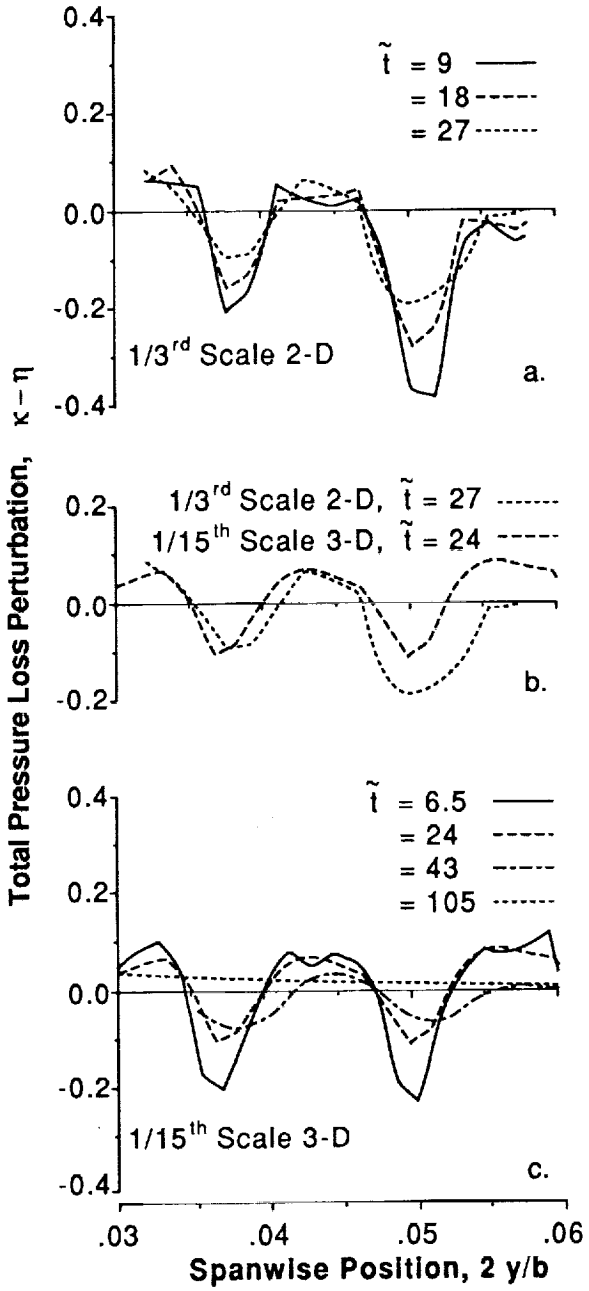

Figure 21. Comparison of large- and small-scale mean wake profiles.

The downstream decay rate of $\overline{u'}$ agrees well with the power law for $\tilde{t} > 20$ up to the beginning of the test section. As the flow enters the test section the rate of decay decreases and departs from the predicted power-law behavior. The ability to extrapolate near-field measurements of $\overline{u'}$ using a power-law function and an empirically

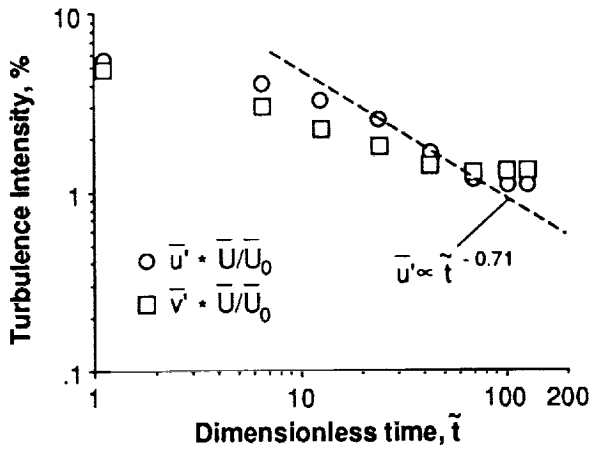

Figure 22. Axial and lateral turbulence intensities on the centerline of the 1/15 scale model's contraction.

derived exponent to predict a test-section turbulence intensity of $\overline{u'}$ = 0.8%, compared to a measured value of $\overline{u'}$ = 1.1%, is adequate for preliminary analysis, and justifies the assumption stated above. The $\overline{u'}$ error of 0.3% underpredicted, based on a constant flow area, is reduced to less than 0.1% at the test section when the inlet's effective contraction ratio of $\overline{U}_0/\overline{U}_{TS}$ = 0.275 (fig. 12) is applied to the data. Although this error is significant when compared to the design goal of 0.5%, the estimate is accurate enough to be used in a preliminary analysis as was done for the baseline vane set.

The correlation between studies using circular rods and the measured behavior of $\overline{v'}$ is less satisfactory. For values of $\tilde{t} > 20$, $\overline{u'}$ decays at the same rate as circular rods, $n = -0.71$, up to the transition between contraction and test section, $\tilde{t} = 104$. Lateral turbulence intensity is observed to decay at a much slower rate. A curve fit of the $\overline{v'}$ data results in an exponential value of $n = -0.44$ compared to $n = -0.66$ reported for circular rod wakes (ref. 22).

The flattening of the decay curves as the flow enters the test section, $\tilde{t} = 104$, is an unexpected anomaly in $\overline{u'}$ and $\overline{v'}$ decay. This is an example of how full 3-D modeling can detect behavior not predicted by 2-D or idealized studies.

An important difference between the 2-D and 3-D behavior of turbulence decay can also be seen in the near-field measurements of $\overline{u'}$. Values of $\overline{u'}$ for both 1/3 and 1/15 scale models are plotted versus dimensionless time, $\tilde{t}$, in figure 23. For this comparison, $\overline{u'}$ from the 1/15 scale model is scaled by the local mean velocity, $\overline{U}$, and the 1/3 scale data has been reduced by a factor of $\overline{U}_0/\overline{U}$ to simulate the effect of accelerated mean flow in

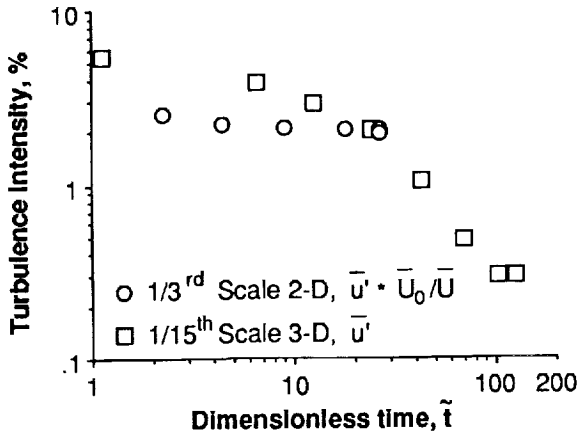

Figure 23. Centerline axial turbulence intensities downstream of the 1/3 and 1/15 scale models.

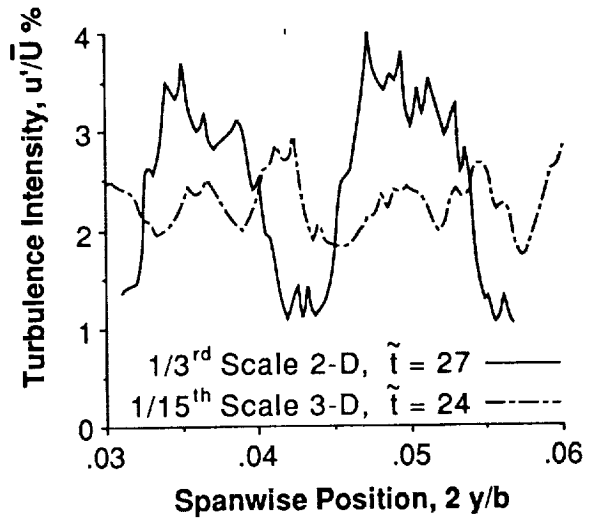

Figure 24. Comparison of large- and small-scale wake turbulence profiles.

the contraction, not present in the 2-D data, to allow direct comparison.

The 1/15 scale measurements of $\overline{u'}$ start at a higher level than the 1/3 scale data, but decay more rapidly. It is believed that these differences are due to the presence of the horizontal splitter plates in the 1/15 scale model. The wakes shed from the splitter plates add more turbulent energy to the flow, increasing initial levels of $\overline{u'}$, and provide enhanced mixing and interaction between the wakes.

The significance of this mixing can be seen by comparing large and small-scale measurements of $u'/\overline{U}$ at the stations $\tilde{t} = 27$ and $\tilde{t} = 24$ (fig. 24). Although the averaged values of $\overline{u'}$ are very close, there is a difference in the distribution of $u'/\overline{U}$ across the profiles. The accelerated mixing of the wakes caused by the splitter plates contributes to a lateral redistribution of turbulence. Measurements of $v'/\overline{U}$ wake profiles show the same trends. This redistribution allows the small-scale data to develop to a more homogeneous state than the large-scale data in the same amount of time. The more rapid decay rate of the 1/15 scale data is to be expected since a homogeneous flow field generally marks the end of turbulence production and the onset of the initial period of decay. In terms of modeling the global mixing process and spatial distribution of turbulence, it appears that the 1/15 scale 3-D data is a closer representation of the full-scale wind tunnel than the 1/3 scale 2-D data.

Full-Scale Wind Tunnel Data

After completion of all facility modifications, the 80- by 120-Foot Wind Tunnel was brought on line and a test-section flow quality investigation conducted. During this test, discrete measurements of $u'/\overline{U}$ and $v'/\overline{U}$ were made in the test section for various external ambient wind conditions. Values of $u'/\overline{U}$ for three spanwise stations and $v'/\overline{U}$ on tunnel centerline, measured with low external wind conditions, are plotted in figure 25. Also plotted for comparison are test section lateral surveys of $u'/\overline{U}$ and $v'/\overline{U}$ from the 1/15 scale model.

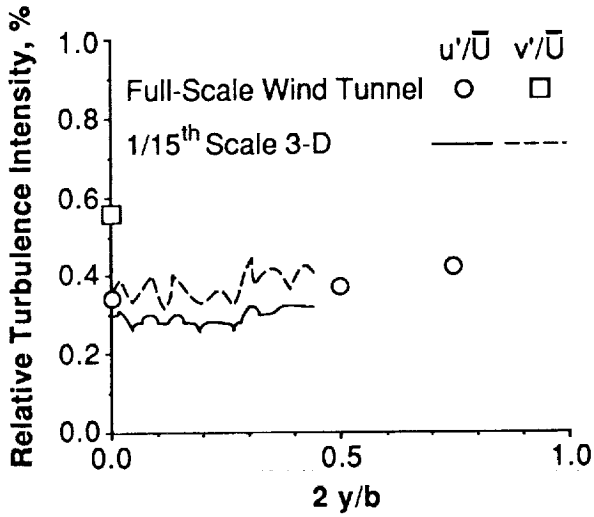

Figure 25. Comparison of small-scale and full-scale wind tunnel test section turbulence intensities.

The large- and small-scale measurements of $u'/\overline{U}$ are in good agreement. Full-scale measurements of $v'/\overline{U}$ were higher than expected and slightly exceeded the design goal of 0.5%.

The trend of increasing turbulence intensity with spanwise position, ϕ, detected during the 1/3 and 1/15 scale tests is also observed full-scale.

Vane Set Total Pressure Loss

The two flow characteristics of greatest interest in these investigations are the turbulence field downstream of the vane set, discussed previously, and the reduction in flow potential energy (total pressure) caused by the vane set. Pressure loss mechanisms are of interest for two reasons. First, the ability of the vane set to isolate the internal flow from atmospheric turbulence depends on the amount of damping that occurs as a result of the head loss generated by the vane set. Second, details of the turbulence field generated are strongly influenced by the pressure loss mechanisms involved. The intent here is to document the relative magnitudes of, and methods used to determine, factors that contribute to the vane set losses. As mentioned previously, this information was used as empirical inputs to analytical predictions of the mean flow distribution in the inlet contraction (ref. 8).

The mechanisms that significantly contribute to vane-set total pressure loss are skin friction, screen head loss, vane boattail base pressure, and wake losses. To simplify analysis, the last two items are lumped together as boattail diffuser losses, the losses associated with diffusing the flow in the passage between boattails of two adjacent vanes. Total pressure loss for each component is expressed in terms of incremental pressure loss coefficients, $\Delta\eta$, where η is the same as defined earlier in this paper. Values of $\Delta\eta$ are shown in table 1.

TABLE 1
Incremental pressure loss coefficients, $\Delta\eta$, for vane components

Component		$\Delta\eta$
Skin Friction	Smooth Surface	0.11
	Perforated Surface	0.17
Screens	Leading Edge	0.30
	Trailing Edge	1.65
Diffuser	Smooth Surface	0.42
	Perforated Surface	0.45

The pressure loss increments listed in table 1 are based on experimental data obtained during the 1/3 scale model investigation. Because of the techniques used, measured values of η include the losses of all components installed for a particular vane set configuration. The losses for the individual components, $\Delta\eta$ listed in table 1, were determined in the following manner. Skin friction loss for smooth vanes was calculated from boundary layer measurements. The loss due to the addition of perforated sides was determined by both boundary layer measurements and the incremental change η when the rough sides were added. Leading and trailing edge screen losses were also determined by incremental changes in η when screens were added or removed. Diffuser losses are taken to be the measured value of η for a particular vane set configuration, minus the skin friction and screen increments. Repeatability of all $\Delta\eta$ measurements was found to be ≈ 0.02 for various combinations of vane set components.

For the purposes of these investigations, only the frictional loss that occurs in the constant area section between the vanes is defined to be skin friction loss. For accounting purposes, boattail skin friction is included with diffuser losses. The values of skin friction loss for the smooth and rough wall surfaces was calculated from measurements of boundary layer velocity profiles at the end of the constant area section (denoted by the subscript 1). These profiles (fig. 26) were numerically integrated to obtain the boundary layer displacement thickness, δ^*, and momentum thickness, δ^{**}, according to

$$\delta^* = \frac{1}{U_1}\int_0^\delta (U_1 - u)\,dy$$

and

$$\delta^{**} = \frac{1}{U_1{}^2}\int_0^\delta u(U_1 - u)\,dy$$

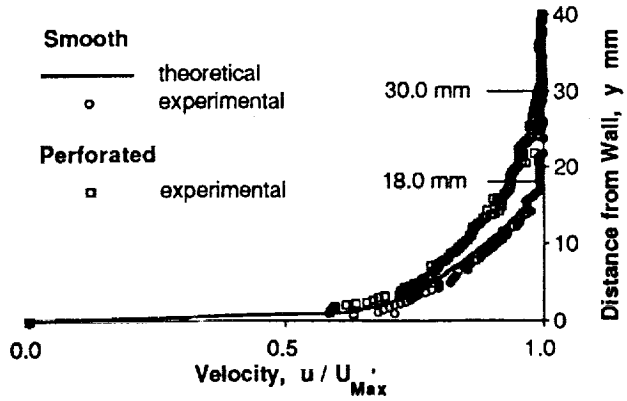

Figure 26. Vane wall boundary layer velocity profiles.

Boundary layer thickness, δ, can be read directly from figure 26, and was 18.0 mm for the smooth surface and 30.0 mm for the perforated surface. Displacement and momentum thickness were calculated to be $\delta^* = 2.7$ mm and $\delta^{**} = 1.8$ mm for a smooth vane surface; for a perforated surface $\delta^* = 4.2$ mm and $\delta^{**} = 2.9$ mm, table 2. It should be noted that the boundary layer profile for the smooth surface is in very close agreement with the theoretical turbulent boundary layer calculated by the law of the wake equation (ref. 27) for a smooth surface at the same Reynolds number.

TABLE 2
Boundary layer parameters (mm)

	δ	δ^*	δ^{**}	c_f
Law of the Wake	18.9	2.6	1.9	0.00310
Smooth Surface	18.0	2.7	1.8	0.00281
Perforated Surface	30.0	4.2	2.9	0.00460

Frictional losses for a vane's unit vertical span were determined from skin friction coefficients based on boundary layer momentum thickness, (conservation of momentum) (ref. 17). The drag due to skin friction was converted into incremental pressure loss coefficients by dividing the drag by the upstream reference dynamic pressure, q_0, and a unit vertical span of flow area at that station. The lateral boundaries of this control volume flow area are defined by the stagnation streamlines that pass along the vane surface generating the drag. The approximation used for stagnation streamline lateral spacing is the vane spacing, l_0.

The pressure loss coefficient increments computed for smooth and perforated surfaces were 0.11 and 0.17 respectively. The 0.17 value is also in good agreement with the incremental change in η when perforated surfaces are added to the vanes. At the Reynolds number tested, for a surface to be considered smooth, the roughness must be less than 0.02 mm. The magnitude of the roughness due to surface perforations, in terms of equivalent sand height is 0.13 mm. This estimated by charted values of c_f as a function of sand height (ref. 17). Although this is less than the perforation depth (sheet thickness) of 0.607 mm, it is well above the admissible roughness of 0.02 mm. This confirms that the observed increases in δ, c_f, and η are caused by surface roughness.

Pressure loss coefficients associated with the trailing edge screens installed in the 1/3 and 1/15 scale models were measured in a component test rig with a constant area duct. Screen samples were installed spanning the entire duct and normal to the flow and tested over a range of Reynolds numbers, Re_d, based on screen diameter. Above a critical Reynolds number range of $300 < Re_d < 600$, loss coefficient was constant at $\eta \approx 1.60$ for both screens (fig. 27). During the 1/3 scale test the screen operated at $Re_d > 3000$, well above critical. For the 1/15 scale test, $Re_d \approx 350$.

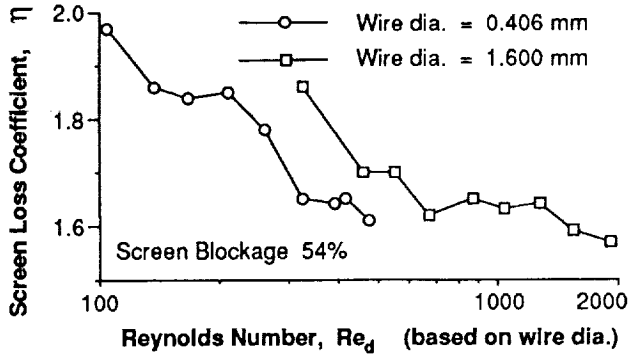

Figure 27. Trailing edge screen pressure loss coefficients.

The difference between $\eta = 1.60$ for an isolated screen and $\eta = 1.65$ for a screen in the presence of the vane set and can be attributed to the non-uniform velocity at the vane set trailing edge. Since the pressure losses are proportional $(U/\overline{U})^2$ rather than $U/\overline{U}$, a non-uniform velocity distribution will always produce greater losses than a uniform flow. An estimate of the expected increase can be made if the velocity distribution of $U/\overline{U}$ at the vane set trailing edge ($\bar{t} = 0.07$ in fig. 16) is approximated by a sawtooth function with maxima of 1.6 at $y/l_0 = 0$, and minima of 0.6 at $y/l_0 = \pm 0.5$. Integrating the square of this function over ± 0.5 y/l_0 indicates the actual average dynamic pressure at the vane set trailing edge, $\overline{q}_0$, would be 5% higher than $\overline{q}_0$ for a uniform flow. This is very close to the difference in the measured values of $\Delta\eta$ for the trailing edge screens.

The diffuser losses measured were found to be slightly less than would be predicted using the methods of reference 26, for a straight wall diffuser with the same geometry and throat blockage. Predicted diffuser $\Delta\eta$'s were between 0.60 and 0.65, compared to measured values of 0.42 to 0.45.

CONCLUDING REMARKS

This study has shown that the combination of large- and small-scale investigations was an effective method of modeling the 80- by 120-Foot

Wind Tunnel's inlet. By combining the results to the two tests, it was possible to deduce information that could not be determined by either test alone. The large-scale model provided a detailed measurements of pressure loss and turbulence generation mechanisms, while the small-scale model allowed a global view of the inlet's behavior.

Comparisons between the results of the two tests established the fidelity of the small-scale model in terms of its ability to match the large-scale flow properties. This matching was facilitated by the adoption of the dimensionless time parameter, $\tilde{t}$, as a means of defining downstream position. The prediction of test-section turbulence intensity based on measurements in the 1/15 scale model were in good agreement with measurements made in the full-scale wind tunnel and verified that the model was of sufficient scale to do meaningful work.

In addition to the predictions of test section turbulence levels, several interesting phenomena were observed in these studies. They include a measured effective contraction velocity ratio of 3.6:1 for an inlet with an area ratio of 5:1, increased levels of turbulence intensity with spanwise position, and differences in turbulence homogeneity at similar downstream positions between the two tests.

The measurements of incremental contributions to the vane set head loss provided useful inputs to other investigations and analyses. Knowledge of the relative contribution of each component is also useful for assessing aerodynamic trade and structural design. The zero-lift drag or head loss of the baseline vane without screens was determined to be less than 25% of the total loss. The increase in vane drag due to surface roughness was measurable, but was not found to have a significant effect on overall vane performance.

The two areas of greatest weakness in the modeling techniques used were the scaling of screen geometry and matching of vane diffuser throat boundary layers. A 1/3 scale screen for the 2-D test would have a six instead of two wire per cm mesh. This would have provided a better model of the full-scale wind tunnel ratio of turbulence scales generated by the vane wake and screen mesh. This ratio is known to have an effect on the rate of turbulence decay. The 1/15 scale model screen was not properly scaled due to higher loss coefficients that would have resulted at the lower Reynolds numbers if a finer mesh screen was used. Ironically, the 1/15 scale test measurements and comments in the literature indicate that the 20:1 wire-to-vane thickness ratio used in the small-scale investigation does a better job of promoting turbulence decay than the 60:1 ratio that exists at full-scale. This leads to the recommendation that vane cascades of this type use a coarser trailing edge treatment with the same blockage and a mesh to vane thickness ratio closer to 5:1. Suitable treatments other than screens would be a biplaner lattice, colander plate, or expanded metal sheets.

Another recommendation to improve the testing techniques for these types of investigations would be to achieve a better match of the diffuser throat blockage parameter due to boundary layer displacement thickness, $2\,\delta^*$ divided by the throat width. For the 1/3 scale investigation this would have required testing the vanes at a Reynolds number 1/3 of full-scale. The matching of this parameter in the 1/15 scale model could have been improved by some simulation of surface roughness.

REFERENCES

1. Snyder, C. T.; and Presley, L. L.: Current Wind Tunnel Capability and Planned Improvements at NASA Ames Research Center. AIAA Paper 86-0729, Mar. 1986.

2. Baals, D. D.; and Corliss, W. R.: Wind Tunnels of NASA. NASA SP-440, 1981.

3. Corsiglia, V.; Olson, L. E.; and Falarski, M. D.: Aerodynamic Characteristics of the 40 × 80; 80 × 120 FT Wind Tunnel at NASA-Ames Research Center. AIAA Paper 84-0601, Mar. 1984.

4. Schmidt, G. I.; Rossow, V. J.; van Aken, J.; and Parrish, C. L.: One-Fiftieth Scale Model Studies of 40- by 80-Foot and 80- by 120-Foot Wind Tunnel Complex at NASA Ames Research Center. NASA TM-89405, 1987.

5. Dudley, M. R.; Unnever, G.; and Regan, D. R.: Two-Dimensional Wake Characteristics of Inlet Vanes for Open-Circuit Wind Tunnels. AIAA Paper 84-0604, Mar. 1984.

6. Soderman, P. T.; Unnever, G.; and Dudley, M. R.: Effects of Boattail Geometry on the Aeroacoustics of Parallel Baffles in Ducts. NASA TM-85891, 1985.

7. Kaul, U. K.; Ross, J. C.; and Jacocks, J. L.: A Numerical Simulation of the NFAC (National Full-Scale Aerodynamics Complex)

Open-Return Wind Tunnel Inlet Flow. NASA TM-86724, 1985.

8. Ross, J. C.; Olson, L. E.; Meyn, L. A.; and van Aken, J.: A New Design Concept for Indraft Wind Tunnel Inlets with Application to the National Full-Scale Aerodynamics Complex. NASA TM-88226, 1986.

9. van Aken, J.; Ross, J. C.; and Zell, P. T.: Inlet Development for the NFAC 80- by 120-Foot Wind Tunnel. AIAA Paper 88-2528, Mar. 1988.

10. van Aken, J.; and Sheller, N. M.: Experimental Investigation of Inlet Flow-Control Cascades for the NFAC 80- by 120-Foot Indraft Wind Tunnel. AIAA Paper 88-0054, Jan. 1988.

11. Staff: Type 55M10 Instruction Manual, DISA 55M System with 55M10 CTA Standard Bridge, M10. Published by DISA Information Department, DISA Electronics Technical Bulletin Reg. No. 9150A4912, Aug. 1977.

12. Staff: Instruction Manual, DISA 55M System with 55M14 Temperature Compensator Bridge. Published by DISA Information Department, DISA Electronics Technical Bulletin Registration No. 9150A5611, Mar. 1984.

13. Bradshaw, P.; and Johnson, R. F.: Turbulence Measurements with Hot-wire Anemometers. National Physical Laboratory, Notes on Applied Science No. 33, 1963.

14. Champagen, F. H.; and Sleicher, C. A.: Turbulence Measurements with Inclined Hot-wires, Part 1 and 2. J. Fluid Mechanics, vol. 28, 1967.

15. Hoffmann, J. A.: Errors in X-wire Measurements due to Wire Angle and Residual Cooling. ISA ASI 74257 (287-290), 1974.

16. Comte-Bellot, G.; and Corrsin, S.: The Use of a Contraction to Improve the Isotropy of Grid-Generated Turbulence. J. Fluid Mechanics, vol. 25, 1965, pp. 657-682.

17. Schlichting, H.: Boundary Layer Theory. 6th ed. McGraw-Hill Book Co., New York, 1968.

18. Hoffmann, J. A.; Kassir, S. M.; and Larwood, S. M.: The Influence of Free-Stream Turbulence on Turbulent Boundary Layers with Mild Adverse Pressure Gradients. NASA CR-177520, Feb. 1989.

19. Introduction to Design and Performance Data for Diffusers. Sponsored by The Royal Aeronautical Society, Institution of Chemical Engineers, and Institution of Mechanical Engineers, Engineering Sciences Data Number 76027, Nov. 1976.

20. Hinze, J. O.: Turbulence. 2nd ed. McGraw-Hill Book Co., New York, 1959.

21. Baines, W. D.; and Peterson, E. G.: An Investigation of Flow Through Screens. Transactions of the ASME, July 1951, pp. 467-480.

22. Gad-El-Hak, M.; and Corrsin, S.: Measurement of the Nearly Isotropic Turbulence Behind a Uniform Jet Grid. J. Fluid Mechanics, vol. 62, part 1, 1974, pp. 115-143.

23. Ramjee, V.; and Hussain, A. K. M. F.: Influence of the Axisymmetric Contraction Ratio on Free-Stream Turbulence. Transactions of the ASME, Sept. 1976, pp. 506-515.

24. Dryden, H. L.; and Schubauer, G. B.: The Use of Damping Screens for the Reduction of Wind-Tunnel Turbulence. Journal of Aeronautical Sciences, vol. 14, no. 4, Apr. 1947, pp. 221-228.

25. Schubauer, G. B.; and Spangenberg, W. G.: Effect of Screens in Wide-Angle Diffusers. NACA Report 949, 1949.

26. Reneau, L. R.; Johnston, J. P.; and Kline, S. J.: Performance and Design of Straight, Two-Dimensional Diffusers. Transactions of the ASME, Journal of Basic Engineering, Paper No. 66-FE-10, Apr. 1966.

27. Coles, D. E.: The Law of the Wake in the Turbulent Boundary Layer. J. Fluid Mechanics, vol. 1, 1956, pp. 191-226.

NASA
National Aeronautics and Space Administration

Report Documentation Page

1. Report No.	2. Government Accession No.	3. Recipient's Catalog No.
NASA TM-102808		

4. Title and Subtitle
Turbulence and Pressure Loss Characteristics of the Inlet Vanes for the 80- by 120-Foot Wind Tunnel

5. Report Date
October 1990

6. Performing Organization Code

7. Author(s)
Michael R. Dudley

8. Performing Organization Report No.
A-90123

10. Work Unit No.
505-61-71

9. Performing Organization Name and Address
Ames Research Center
Moffett Field, CA 94035-1000

11. Contract or Grant No.

13. Type of Report and Period Covered
Technical Memorandum

12. Sponsoring Agency Name and Address
National Aeronautics and Space Administration
Washington, DC 20546-0001

14. Sponsoring Agency Code

15. Supplementary Notes
Point of Contact: Victor Corsiglia, Ames Research Center, MS 247-2, Moffett Field, CA 94035-1000
(415) 604-6677 or FTS 464-6677

16. Abstract

A series of wind tunnel investigations were conducted at NASA Ames Research Center to determine the flow characteristics downstream of a set of wind tunnel inlet flow conditioning vanes. The purpose of these tests was to develop an understanding of the flow mechanisms that contributed to the pressure loss and turbulence generated by the vane set. The near-field characteristics and flow field development were investigated with a 1/3 scale two-dimensional model of the vane set at near full-scale Reynolds numbers. In a second series of tests, the global flow field characteristics were investigated by means of a 1/15 scale model of the full vane set and the 5:1 contraction leading to the model's test section. Scale effects due to Reynolds number mismatch were identified, their significance noted and accounted for when possible. Scaling parameters were adopted that allowed predictions of the expected turbulence and pressure distributions in the full-scale wind tunnel test section, based on the small-scale test results. The predictions were found to be in good agreement with actual measurements made in the full-scale facility.

17. Key Words (Suggested by Author(s))	18. Distribution Statement
Wind tunnel inlet Vane Cascade Turbulence	Unclassified-Unlimited Subject Category - 09

19. Security Classif. (of this report)	20. Security Classif. (of this page)	21. No. of Pages	22. Price
Unclassified	Unclassified	23	A01

For sale by the National Technical Information Service, Springfield, Virginia 22161